Cerebral Cortex September 2007;17:2007–2018
doi:10.1093/cercor/bhl109
Advance Access publication November 6, 2006

Reduced Neocortical Thickness and Complexity Mapped in Mesial Temporal Lobe Epilepsy with Hippocampal Sclerosis

Jack J. Lin[1], Noriko Salamon[2], Agatha D. Lee[3], Rebecca A. Dutton[3], Jennifer A. Geaga[3], Kiralee M. Hayashi[3], Eileen Luders[3], Arthur W. Toga[3], Jerome Engel, Jr[1,4,5] and Paul M. Thompson[3]

[1]Department of Neurology, [2]Department of Radiology, [3]Laboratory of Neuro Imaging, Brain Mapping Division, [4]Department of Neurobiology, [5]Brain Research Institute, David Geffen School of Medicine at UCLA, Los Angeles, CA 90095, USA

We mapped the profile of neocortical thickness and complexity in patients with mesial temporal lobe epilepsy (MTLE) and hippocampal sclerosis. Thirty preoperative high-resolution magnetic resonance imaging scans were acquired from 15 right (mean age: 31.9 ± 9.7 standard deviation [SD] years) and 15 left (mean age: 30.8 ± 8.4 SD years) MTLE patients who were seizure-free for 2 years after anteriomesial temporal resection. Nineteen healthy controls were also scanned (mean age: 24.8 ± 3.9 SD years). A cortical pattern matching technique mapped thickness across the entire neocortex. Mesial temporal structures were not included in this analysis. Cortical models were remeshed in frequency space to compute their fractal dimension (surface complexity). Both MTLE groups showed up to 30% bilateral decrease in cortical thickness, in the frontal poles, frontal operculum, orbitofrontal, lateral temporal, and occipital regions. In both groups, cortical complexity was decreased in multiple lobar regions. Significant linkages were found relating longer duration of epilepsy to greater cortical thickness reduction in the superior frontal and parahippocampal gyrus ipsilateral to the side of seizure onset. The pervasive extrahippocampal structural deficits may result from chronic seizure propagation or may reflect other causes such as initial precipitating factors leading to MTLE.

Keywords: brain-mapping, cortical complexity, cortical thickness, mesial temporal lobe epilepsy, MRI

Introduction

Mesial temporal lobe epilepsy (MTLE) is the most frequent form of drug-resistant epilepsy and is commonly associated with hippocampal sclerosis (HS) (Babb et al. 1984). There is convergent evidence that MTLE patients have functional and structural abnormalities that extend beyond the hippocampus. Neuropsychological morbidities associated with MTLE extend beyond the memory systems and involve additional cortical domains such as intellectual function, language, executive function, and motor speed (Oyegbile et al. 2004). Flumazenil and fluorodeoxyglucose Positron Emission Tomography studies have demonstrated metabolic disturbances in neocortical areas (Henry et al. 1993; Hammers et al. 2001). Recently, there has been an increased interest in investigating extrahippocampal structural abnormalities in MTLE patients. Some investigators have used region-specific protocols to detect structural abnormalities in neocortical temporal lobe and parahippocampal regions (Moran et al. 2001; Bernasconi et al. 2003). Voxel-based morphometric methods have been developed to detect structural changes throughout the entire brain without a priori assumptions of the specific regions of interest. Despite varying results that may stem from differences in normalization techniques or cohort differences, reductions in gray matter concentration have been reported in the neocortical frontal, temporal, and parietal-occipital regions (Keller et al. 2002; Bernasconi et al. 2004; Bonilha et al. 2004).

Voxel-based morphometry (VBM) quantifies group differences observed in "gray matter density" (Wright et al. 1995; Bullmore et al. 1999). Gray matter density measures the proportion of voxels in small regions of the brain that are classified as gray matter compared with voxels representing other tissue types such as white matter and cerebrospinal fluid (CSF). As such, gray matter density is sensitive to both losses in gray matter as well as increases in CSF volume, as well as differences in cortical surface curvature, which cannot be distinguished from each other. Advances in brain image analysis have made it possible to estimate gray matter cortical thickness in millimeters, from T_1-weighted magnetic resonance imaging (MRI) scans (Fischl and Dale 2000; Jones et al. 2000; MacDonald et al. 2000; Miller et al. 2000; Kruggel et al. 2001; Yezzi and Prince 2001; Annese et al. 2002; Lerch and Evans 2005). We recently developed such a method to measure cortical thickness throughout the brain volume at submillimeter accuracy (Narr et al. 2005; Sowell et al. 2004; Thompson, Hayashi, Sowell, et al. 2004, Thompson et al. 2005; Luders, Narr, Thompson, Rex, Jancke, et al. 2006; Luders, Narr, Thompson, Rex, Woods, et al. 2006). This method detects changes in the cerebral neocortex and thus does not analyze subcortical structures including mesial temporal structures. During the prenatal period, cells migrate from the marginal zone to the telencephalon resulting in increased cortical thickness. The gray matter thickness ranges from 1.5 to 4.5 mm in the adult brain and primarily reflects the packing density and arrangement of neuronal cells. Measurement of the thickness of the cortical mantle over the entire cortical surface may offer a more sensitive way to evaluate cortical structural disturbances in patients with chronic drug-resistant temporal lobe epilepsy (TLE). In addition, thickness measures are more specific in that they are sensitive to cortical thinning exclusively, rather than a mixture of gray matter loss, CSF gain, and cortical curvature differences, which confounds the interpretation of measures based on gray matter density (Narr et al. 2005).

In addition to mapping cortical thickness, we also aimed to study gyrification patterns in MTLE. Although gyral formation begins at approximately 16 weeks in utero, most of the cortical convolutions are formed during the late second and third trimester of pregnancy (Armstrong et al. 1995). Postnatally, human cortical gyral complexity remains fairly stable, although moderate increases in gyral complexity have been observed during childhood (Blanton et al. 2000). Disease processes that disrupt underlying cortical connections may lead to disturbances in gyrification (Rakic 1988). To quantify changes in cortical folding patterns associated with MTLE, we applied an algorithm

that we recently developed to measure gyral complexity in 3D (Thompson et al. 2005), using high-resolution cortical surface models extracted from each subject's MRI.

In this study, we set out to determine whether patients with drug-resistant MTLE have regional-specific changes in cortical thickness and to quantify cortical gyral complexity in this epilepsy syndrome. We used cortical asymmetry maps to determine the association between the side of seizure onset and cortical deficit patterns. We also related selective profiles of brain structure changes to clinical variables including duration of epilepsy, seizure frequency, history of febrile seizures, and antiepileptic medication history (i.e., the number of ineffective antiepileptic drugs patients experienced in their lifetime).

Patients and Methods

Patients

Using the University of California, Los Angeles, adult epilepsy surgical database (1993–2002), we retrospectively identified 15 patients with right mesial temporal lobe epilepsy (RMTLE, mean age: 31.9 ± 9.7 standard deviation [SD] years, age range: 19–48), 15 patients with left mesial temporal lobe epilepsy (LMTLE, mean age: 30.8 ± 8.4 SD years, age range: 18–40), and 19 healthy young adult controls (mean age: 24.8 ± 3.9 SD years, age range: 18–26). Within the epilepsy patient group, MRI studies were grouped according to the side of HS and compared with the healthy control group. The diagnosis of unilateral MTLE was based on clinical, neuroimaging, electrophysiological, and pathological criteria. For inclusion, patients were required to have a history of simple partial seizures or complex partial seizures or both, with semiology compatible with mesial temporal lobe origin. Preoperative MRI must demonstrate unilateral or asymmetric hippocampal atrophy with increased T_2 signal consistent with HS and verified by a board certified neuroradiologist (N.S.). All patients had noninvasive ictal electroencephalography revealing at least 3 seizures with unilateral temporal lobe onset, concordant with the side of hippocampal atrophy on MRI. Surgical pathology was required to show evidence of HS. Patients with MRI or pathological abnormalities other than HS were excluded. All patients had undergone standard en bloc anteromesial temporal resection, as described by Spencer et al. (1984), by a single neurosurgeon. A clinical nurse specialist conducted telephone interviews every 2–3 months after the surgery for at least 2 years to determine patients' seizure frequency. All patients were free of disabling seizures except for aura in isolation (Engel Class I outcome) and had been maintained on antiepileptic medications for at least 2 years. Patient characteristics are detailed in Table 1.

Table 1
Patient characteristics

Clinical features	RMTLE, n = 15	LMTLE, n = 15
Age at MRI scan (years)	31.9 ± 9.7	30.8 ± 8.4
Gender M/F	4/11	10/5
Age at first seizure onset (years)	13.2 ± 10.1	11.4 ± 7.8
Epilepsy duration (years)	19.2 ± 9.9	20.0 ± 10.6
Number of ineffective AEDs tried	5.67 ± 0.42	5.06 ± 0.48
Seizure frequency (per month)	7.9 ± 5.5	10.1 ± 6.6
History febrile seizures (%)[a]	40	40
History of CNS infection (%)[a]	7	20
History of head trauma (%)[a]	20	13

Note: Data are shown as mean ± standard error of the mean; M = male, F = female; R = right, L = left; AED = antiepileptic drug.
[a]Percent of total subjects.

MRI Scans

High-resolution MRI images were acquired on a GE Signa 1.5-T clinical scanner (Milwaukee, WI). For epilepsy patients, whole-brain preoperative T_1-weighted images were acquired during the course of their clinical evaluation. Using spoiled gradient recalled acquisition in steady state (SPGR) to resolve anatomy at high resolution, a series of 124 contiguous 1.8 mm coronal brain slices were obtained with the following parameters: 256 × 256 matrix, 0.98 mm × 0.98 mm in-plane resolution. Because the MRI scans were initially collected in patients for clinical purposes, a different protocol was used to collect the scans in the healthy control group. A series of 124 contiguous 1.5-mm coronal SPGR anatomical MRI scans was obtained using the following parameters: 256 × 256 matrix, 0.98 mm × 0.98 mm in-plane resolution.

Effects of Different Scanner Protocols

In order to evaluate the effects of different scanner protocols on gray matter volumes, a control subject from the original control cohort was rescanned using the same MR scanner and protocol as the epilepsy patients. Automated tissue segmentation was performed on the image data and nonbrain tissues such as scalp and orbits were removed as detailed previously (Shattuck et al. 2001). Total (TGM) and hemispheric gray matter (HGM) volumes were calculated for the original scan (S1) and the repeat scan (S2). S2 showed approximately 10% more gray matter volume than S1 (TGM S1 = 566 874 mm^3, S2 = 633 793 mm^3; right HGM S1 = 279 262 mm^3, S2 = 312 985 mm^3; left HGM S1 = 287 070 mm^3, S2 = 319 834 mm^3). Therefore, this individual difference attributable to different scanner protocols is around 10%. Because we scanned 19 controls, the individual differences of 10%, if they were systematic, would translate into a mean error of the order of [10/sqrt(N – 1)] or around 2.3% in mean gray matter volume between groups. In addition, the S2 scanner, in which the patients' scans were obtained, produced a slight increase in gray matter volume, which will bias against finding a difference in the epilepsy groups. Further, scanner effects were not a potential confound for the maps reporting asymmetries in patients, as both hemispheres were scanned in the same image and all patients were scanned on the same scanner.

Image Processing

Each image volume was linearly aligned and manually registered to a standard orientation by an image analyst (J.J.L.) who "tagged" 20 standardized anatomical landmarks in each subject's image data set to the identical 20 anatomical landmarks defined on the International Consortium on Brain Mapping 53 average brain (ICBM-53). This step was performed in order to reorient each brain volume into the standardized coordinate system of the ICBM-53 average brain, correcting for differences in head tilt and alignment between subjects but leaving scale differences intact. The ICBM-53 template was chosen for this step because compared with other templates (i.e., ICBM-152), the ICBM-53 has slightly better contrast and more sharply defined anatomical features. However, the choice of template will likely to have minimal effect because all ICBM templates are linearly coregistered and reside in the same canonical anatomical space. Because only linear registration of subject data was used in this step, the only determining features that affect the analysis are related to the overall size of the template. The improved anatomical resolution in ICBM-53 may allow more accurate registration of individual brain volume to the template but is in the canonical space of the other ICBM templates that have been used as standards for anatomical normalization. The next step more carefully spatially registered brain volumes to each other using 144 standardized, individually manually defined anatomical landmarks, representing the endpoints of the cortical sulci. These 72 landmarks in each hemisphere represent first and last

points on each of the 36 sulcal lines drawn in each hemisphere as described previously (Thompson et al. 2005). Individual brain images were spatially matched to a set of average cortical landmarks derived for the healthy controls with a least squares, rigid-body transformation. This procedure allows each individual's brain to be matched in a common space but keeps global differences in brain size and shape intact. Automated tissue segmentation was performed on each data set to classify voxels based on signal intensity as most representative of gray matter, white matter, CSF, or extracerebral background class (Thompson et al. 2005). A Gaussian mixture distribution reflecting the statistical variability of intensities in each image was first computed before assigning each voxel to the class with the highest probability (Shattuck et al. 2001). Gray and white matter tissues were retained for further analysis, whereas nonbrain tissue such as scalp and orbits were removed from the spatially transformed, tissue-segmented images. A three-dimensional cortical surface model was extracted with automatic software by creating a mesh-like surface that is continuously deformed to fit a threshold intensity value of the brain image that best differentiates cortical CSF from underlying cortical gray matter (Thompson, Hayashi, Simon, et al. 2004).

Cortical Pattern Matching

An image analysis method known as cortical pattern matching (Thompson, Hayashi, Simon, et al. 2004) was employed to spatially relate thickness information from homologous cortical areas across subjects. By explicitly matching cortical gyral patterns, this technique eliminates much of the confounding anatomical variance when pooling data across subjects and increases the power to detect group differences. A set of 72 sulcal landmarks per brain was used to constrain the mapping of one cortex onto another. Image analysts (A.D.L. and R.A.D.) traced 17 sulci on the lateral and 13 sulci on the medial surface of each hemisphere. On the lateral brain surface, these included the Sylvian fissure, central, precentral, and postcentral sulci, superior temporal sulcus (STS) main body, STS ascending branch, STS posterior branch, primary and secondary intermediate sulci, inferior temporal, superior and inferior frontal, intraparietal, transverse occipital, olfactory, occipitotemporal, and collateral sulci. On the medial surface, these included the callosal sulcus, the inferior callosal outline, the paracentral sulcus, anterior and posterior cingulate sulci, the outer segment of a double parallel cingulate sulcus (where present; see Ono et al. 1990), the superior and inferior rostral sulci, the parietooccipital sulcus, the anterior and posterior calcarine sulci, and the subparietal sulcus. In addition to contouring the major sulci, a set of 6 midline landmark curves bordering the longitudinal fissure was outlined in each hemisphere to establish hemispheric gyral limits. These landmarks specified above were defined according to a detailed anatomical protocol based on the Ono (1990) sulcal atlas. To establish interrater reliability, the cortical sulcal lines were drawn independently on 6 test brains. The raters' sulcal tracings were compared with a set of template sulcal lines with previously established high interrater reliability (Sowell et al. 2002). Differences in millimeters between the two sets of tracings at 100 equidistant points were compared to confirm that the average disparity is within 3.5 mm of the template sulcal delineations. This protocol is available on the Internet (Hayashi et al. 2002, http://www.loni.ucla.edu/~khayashi/Public/medial_surface/).

Cortical Thickness

Figure 1(*a*,*b*) shows steps involved in measuring cortical thickness. To quantify gray matter cortical thickness, we first created average 3D surface models for the MTLE and control groups from the cortical pattern matching algorithms. Points on the cortical surface around and between sulcal landmarks of each individual's brain surface were calculated using the average sulcal contours as anchors to drive the 3D cortical surface models from each subject into correspondence. This results in group average maps in which various features of the brain surface, such as cortical thickness, can be generated. Cortical thickness was defined as the 3D distance measured from the white–gray matter boundary in the tissue classified brain volume to the cortical surface (gray–CSF boundary) in each subject (see Fig. 1). Tissue classified brain volumes were first resampled using tri-linear interpolation to 0.33 mm isotropic voxels in order to obtain distance measures indexing gray matter thickness at subvoxel spatial resolution. Gray matter thickness was measured at thousands of homologous cortical points in each subject in order to quantify the 3D thickness of the cortical ribbon across the entire neocortex. To ensure the accuracy of cortical thickness measures, we compute them in the 3D image volume at a voxel level using gray matter segmentation of the image rather than using the vertices in the surface mesh. Using vertices of a surface mesh to compute cortical thickness may be prone to errors due to departures of the vertices in the surface mesh from the exact 3D interface of gray and white matter or difficulties in defining gray–CSF interface in areas where sulci are narrow. We define the gray–white interface as the voxels classified as gray matter that have at least one neighboring white matter voxel and these voxels are assigned a distance code of zero. In subsequent analysis, successive layers of voxels that are adjacent to the subsequent voxels are coded with values equal to the closest 3D distance to the gray–white interface. These steps compute the shortest distance from a given gray matter voxel and avoid solutions in which this boundary line passes through CSF. A shortcut across white matter would imply that the shortest path has not been found and thus this protocol automatically avoids white matter voxels when assigning gray matter thickness distances. The thickness data were smoothed using a surface-based kernel of 10-mm radius. Spatial filtering is performed on the thickness maps in order to increase the signal to noise ratio. First, smoothing reduces high-frequency noise in the cortical thickness measures by increasing the spatial coherence of the thickness values. Because the cortex is only about 3–6 voxels thick in the original MRI data, replacing individual vertex values with neighborhood averages can reduce noise in the thickness estimate. Second, according to the Central Limit Theorem, filtering increases the residuals after a statistical model is fitted, and improves the power of statistical tests (even though their validity is guaranteed here by permutation testing). Finally, smoothing reduces the effects of imperfect anatomical alignment. Cortical pattern matching greatly reduces cross-subject misregistration of anatomy and the need for a broad smoothing filter. Minimal smoothing increases the sensitivity in detecting regional differences at a small spatial scale. By the matched filter theorem, the optimal filter size should reflect the scale of the signal being detected. Because we expected to find differences at approximately the scale of a gyrus (approximately 10 mm), or in larger regions, we used a 10-mm smoothing kernel. Gray

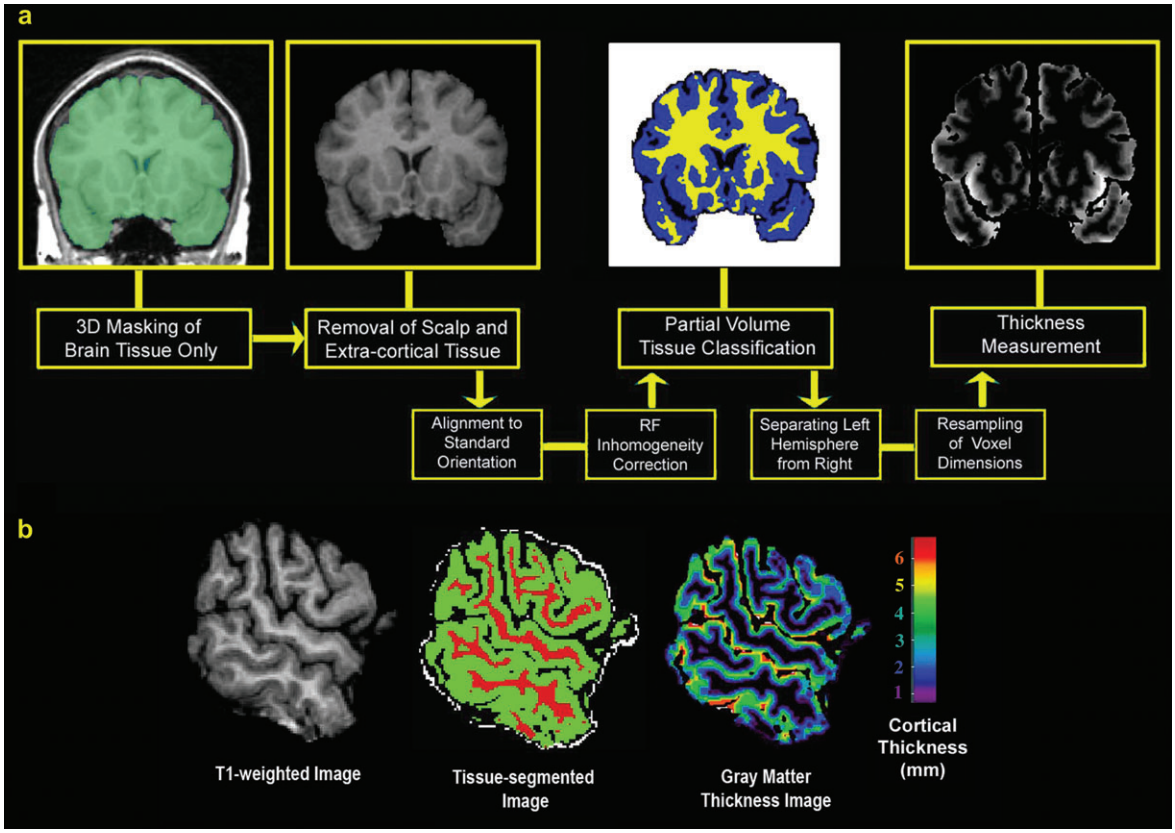

Figure 1. Steps used to generate cortical thickness maps. (*a*) Series of image processing steps required to derive cortical thickness maps from the MRI scans (see Methods session for details). (*b*) A sagittal cut from the original T_1-weighted image for one representative control subject, the tissue-segmented image, and the gray matter thickness image, in which thickness is progressively coded in millimeters from inner to outer layers of cortex using a distance field. RF = radio frequency.

matter thickness was then compared across subjects and averaged at each cortical surface location to produce spatially detailed maps of local thickness differences within and between groups. Cortical matching allows the association of gray matter thickness from homologous regions across subjects by averaging data from homologous gyral regions, using sulcal landmarks as constraints, which would be impossible if data were only linearly mapped to stereotaxic space. This eliminates much of the confounding gyral pattern variability when averaging across individual brain volumes in a data set.

Statistical Maps of Cortical Thickness

Color-coded statistical maps were generated to visualize differences in local gray matter thickness between the MTLE groups and the control group. For this purpose, a regression was performed at each cortical point to assess whether the thickness of the cortical gray matter at that point depended on group membership. The *P* value describing the significance of this linkage was plotted at each point on the neocortex using a color code to produce a significance map. The spatial maps (uncorrected) are crucial for allowing us to visualize the spatial patterns of gray mater deficits but permutation methods were used to assess the overall significance of the statistical maps and to correct for multiple comparison (Bullmore et al. 1999; Nichols and Holmes 2002). A permutation test measures features of the statistical map computed for group differences in cortical thickness when subjects are randomly assigned to groups. Permutation test was performed with a fixed threshold of $P = 0.01$. This statistical level is often used in the brain mapping literature and although other thresholds are possible, our pervious works have used this threshold to detect group differences (Thompson et al. 2005; Luders, Narr, Thompson, Rex, Jancke, et al. 2006; Luders, Narr, Thompson, Rex, Woods, et al. 2006). Other thresholds are possible, and more relaxed thresholds could be used if a more diffuse, weak signal were expected. In a permutation test, the controls and epilepsy patients were randomly assigned to two groups of the same size as the original groups, 100 000 times. Performing a new statistical test on each cortical point for each random assignment generates a null distribution, which represents the area or proportion of the cortex with significant results at voxel level ($P < 0.01$) produced by chance. The area (or proportion) of the cortex that will show significant differences by chance (at the 0.01 significance level) will on average be 1%, in null data. If the observed cortical area with significant thickness differences exceeds those observed by chance in the permutation distribution, then a *P* value is assigned to give a corrected significance value for the observations. The corrected *P* value is simply the proportion of random permutations in which the area of cortex that appears significant exceeds that found in the true assignment of subjects to the patient and control groups. This can be represented symbolically, as follows:

Let the area of the cortex with group differences in cortical thickness exceeding the $P < 0.01$ threshold = A

Then we randomly assigned patients and controls to groups 100 000 times.

Let the proportion of the cortex with significant differences in the random permutations = A_i, in which i = 1 to 100 000, for 100 000 permutations.

Sort the values A_i into numerical order from 0 to 1 and find the rank r of A in the sorted list.

Then r/100 000 is the corrected P value for the permutation test.

Cortical Complexity

Previous methods for measuring gyrification have typically compared the length of an inner and outer contour in 2D MR brain slices (Fig. 2*a* adopted from Zilles et al. 1988; Cook et al. 1995). We also applied an algorithm we recently developed to measure the fractal dimension (complexity) of the human cerebral neocortex in 3D (Luders et al. 2004; Thompson et al. 2005), based on an earlier algorithm developed for mapping the complexity of the deep sulcal surfaces in the brain (Fig. 2*a*; Thompson et al. 1996). The cortex was first divided into 4 separate surface meshes (frontal, temporal, parietal, and occipital regions) in each hemisphere using manually delineated anatomical constraints in order to assess cortical complexity in these 4 distinct neuroanatomic areas (as in Luders et al. 2004). The frontal regions included cortex anterior to the central sulcus. The temporal regions were delimited as the cortex inferior to the Sylvian fissure and posteriorly by a line from the posterior limit of the Sylvian fissure (horizontal ramus) to the posterior extreme of the temporal sulci and collateral sulci on the inferior surface of the brain. The occipital notch was not used as a landmark because it is not reliably distinguishable on the hemispheric surfaces. Parietal regions were defined to include cortex posterior to the central sulci and anterior to the parietal-occipital fissure with temporal region boundaries used as the inferior limits. Occipital regions included cortex bordered by parietal and temporal regions anteriorly. Cortical complexity was defined as the rate at which the surface area of the cortex increases relative to increases in the spatial frequency of the surface model used to represent it. Cortical pattern matching was used to anchor sulcal landmarks to the reparameterized cortex so that corresponding sulci and cortical regions occurred in the same regions of the parameter space across subjects. As in Thompson et al. (2005), the resulting deformed spherical parameterization was discretized in parameter space using a hierarchy of quadtree meshes of size $N \times N$, for N = 2 to 256. The cortex was remeshed at each spatial frequency and its surface area measured (Fig. 2*b*). The rate of increase of surface area with increasing spatial frequency was estimated by least squares fitting of a linear model to the estimated surface area versus frequency, on a log–log plot (Fig. 2*c*; this plot is termed a *multifractal plot* in the fractal literature; see Kiselev et al. 2003, for a discussion of this concept). If $A\{M(N)\}$ represents the surface area of the cortical surface mesh $M(N)$, the fractal dimension or complexity was computed as $\mathrm{Dim}_F = 2 + \{d(A \ln \{M(N)\})/d \ln N\}$. The gradient of the multifractal plot is obtained by regressing $\ln A\{M(N)\}$ against $\ln N$. For a flat surface, this slope is zero, and the dimension is 2; representing the surface at a higher spatial frequency adds no detail. Values above 2 indicate increasing surface detail and greater gyral complexity. Intuitively, higher complexity means the area increases rapidly as finer scale details are included.

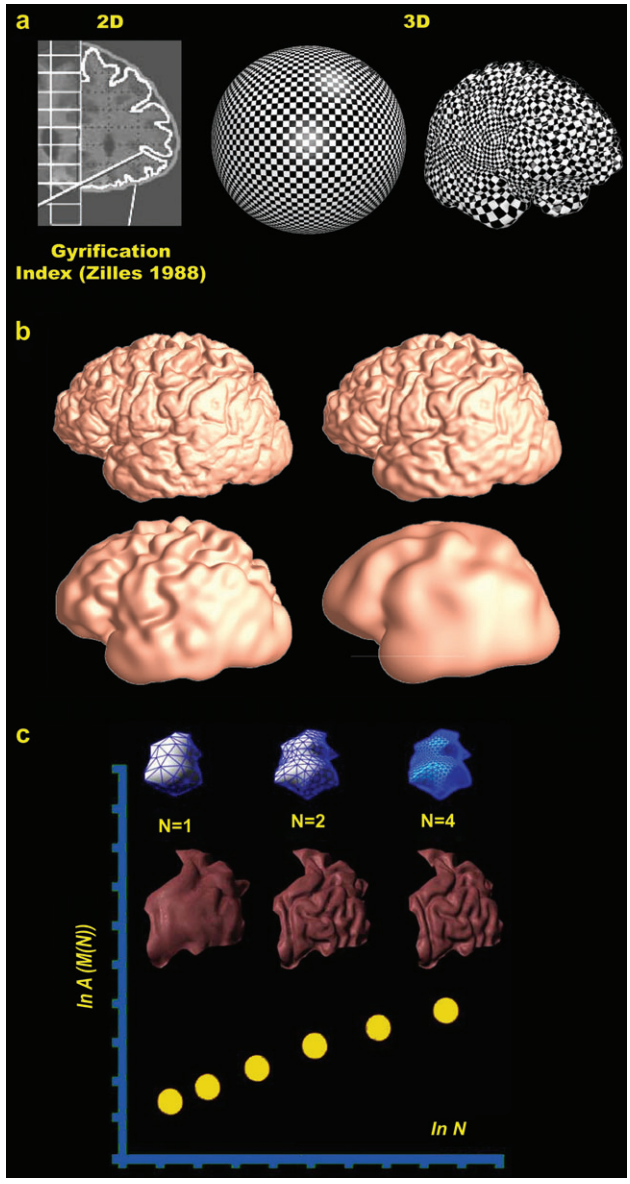

Figure 2. Measuring cortical complexity in three dimensions. Measuring cortical complexity in three dimensions does not depend on the orientation in which the brain is sliced and thus avoid biases associated previous 2D methods such as gyrification index (GI). (*a*) GI measures cortical folding based on a series of MRI sections (adapted from Zilles et al. 1988). The GI compares the boundary of the inner contour of the cortex, following sulcal crevices, with the boundary of the cortical convex hull, which is the convex curve with smallest area that encloses the cortex. The ratio of these is computed and expressed as a weighted mean across slices. Instead, our approach computes complexity from a spherical surface mesh that is deformed onto the cortex. The cortex is then mathematically regridded at successively decreasing frequencies (*b*), such that smoother cortices have less surface area. By plotting the observed surface area versus the cutoff spatial frequency in the surface representation, on a log–log plot (*c*), more complex objects have greater gradients. This plot is called a multifractal plot: the *x*-axis represents the log of number of nodes in the surface grid (here denoted by ln N), and the *y*-axis measures the log of the surface area of the resulting mesh [here denoted by ln $A(M(N))$, where A is the area function and $M(N)$ is the surface mesh with N nodes]. For nonflat surfaces, this plot has a positive slope because the surface area increases as more nodes are included in the mesh. The slope of this plot is added to 2 to get the fractal dimension of the surface (Thompson et al. 1996) (3D figure in *b* and *c* were adapted from Gu et al. 2003). Adding the gradient of the multifractal plot to 2 is a convention used when computing fractal dimensions for surfaces. It ensures that the computed fractal dimension of a flat 2D plane agrees with its Euclidean dimension, which is 2, because the surface is 2D (for details, see Methods).

Regression of Cortical Thickness against Clinical Characteristics

Statistical maps were generated to localize the degree to which cortical thickness was statistically linked to patients' clinical measures. For this purpose, at each cortical point, a multiple regression analysis was run to evaluate whether cortical thickness measures depended on covariates of interest (clinical characteristics listed in Table 1). To increase the power of regression analyses, cortical pattern matching was used to pool together the LMTLE and RMTLE groups according to the side of seizure onset, increasing the number of patients from 15 in each group to a total of 30. The hemispheres were denoted as either ipsilateral or contralateral to the side of seizure onset (Fig. 5). We calculated the average cortical thickness in each hemisphere ipsilateral and contralateral to the side of seizure onset and performed regression of the thickness against these clinical factors at each cortical point. The P value describing the significance of this linkage was plotted at each point on the cortex using a color code to produce a statistical map. Permutation testing was performed to correct for multiple comparisons.

Cortical Asymmetry

The average right and left hemisphere cortical thickness for RMTLE and LMTLE were first created using the methods detailed above. In order to examine asymmetries in each epilepsy group, cortical thickness maps were flipped vertically in midsagittal plane (x = 0). Dividing the average left hemisphere cortical thickness by the corresponding right hemisphere value (after sulcal pattern matching across hemispheres) generated a ratio map of percentage asymmetries. Values greater than 1 indicate that the right hemisphere had lower cortical thickness compared with the left hemisphere; values less than 1 indicate that the left hemisphere had lower cortical thickness compared with the right hemisphere. In an attempt to increase the power of the analysis, we also investigated cortical asymmetry by pooling data ipsilateral and contralateral to the side of seizure onset. Cortical matching was used to pool the 2 patient groups together (N= 30) by transforming the images across the midline plane in order to maintain consistent side of seizure onset, combining data from the side of seizure onset, and also combining data from the hemispheres opposite to that of seizure onset. A ratio of cortical thickness map was computed by dividing the average cortical thickness ipsilateral to the side of seizure onset by the mean map for the contralateral hemisphere. In this map, values greater than 1 would indicate that the contralateral hemisphere had lower cortical thickness, on average, compared with the ipsilateral hemisphere. Permutation tests were performed to evaluate the significance of asymmetries and to correct for multiple comparisons, as described above.

Results

Reduced Cortical Thickness (MTLE vs. Normal)

Compared with healthy controls (Fig. 3*a*), both RMTLE and LMTLE groups showed regions with up to a 30% bilateral decrease in average cortical thickness (denoted in red in Fig. 3*b*,*d*). Significant thinning of the cortical ribbon is visualized in the bilateral frontal poles, frontal operculum, orbital frontal, lateral temporal, and occipital regions. In both MTLE groups, cortical thickness was also reduced in the right angular gyrus and primary sensorimotor cortex surrounding the central sulcus. To measure and map the significance of the decreases in cortical thickness (Fig. 3*c*,*e*), comparisons were made locally between the mean group difference in thickness and an estimate of its standard error at each cortical point. The resulting significance map, corrected for multiple comparisons, showed that cortical thickness reductions in both MTLE groups were highly significant (P < 0.005).

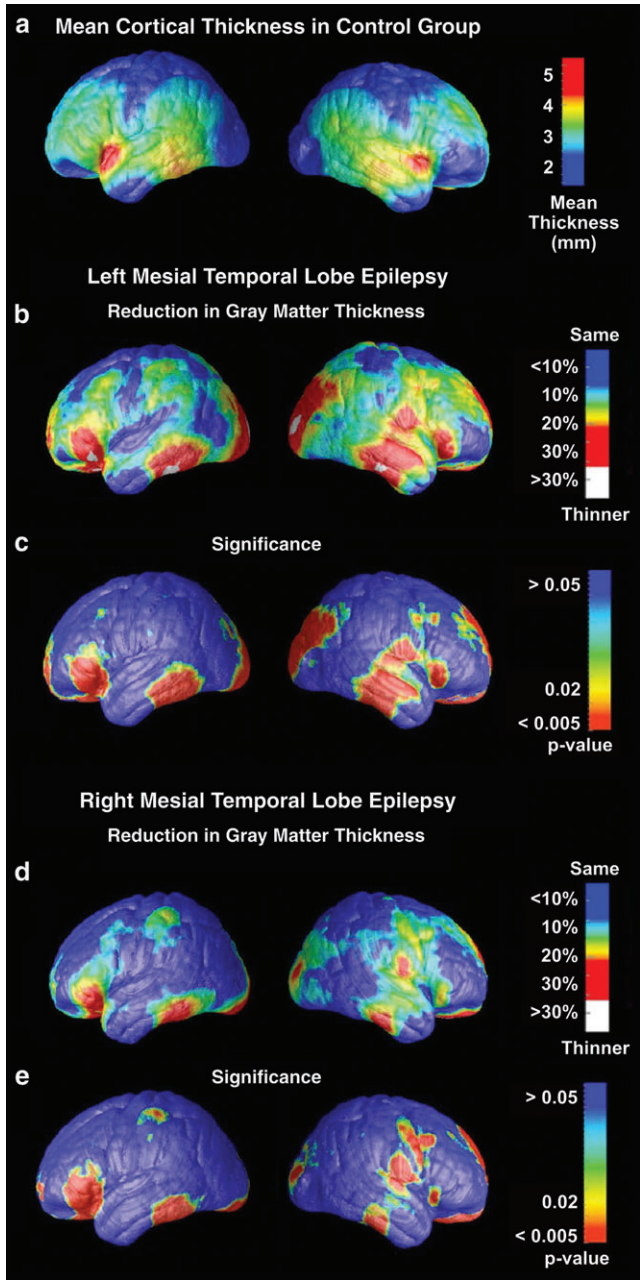

Figure 3. Cortical thickness maps: regional reduction in MTLE groups. The mean cortical thickness for controls (N = 19) is shown on a color-coded scale in (*a*). Cortical thickness is measured in millimeters as shown in the color bar in which red colors indicate a thicker cortex and blue colors indicate a thinner cortex. The mean reduction in cortical thickness in LMTLE and RMTLE groups as a percent of the control average in (*b* and *d*). Red colors in the bilateral in the frontal poles, frontal operculum, orbital frontal, lateral temporal, occipital regions, and the right angular gyrus and primary sensorimotor cortex surrounding the central sulcus denote up to 30% decrease in thickness, on average, compared with corresponding areas in controls. The significance of these changes is shown as a map of P values in (*c* and *e*).

Decreased Cortical Complexity (MTLE vs. Normal)

Statistical comparisons of cortical complexity values revealed significantly decreased cortical complexity in specific lobar regions of both MTLE groups compared with healthy controls (Fig. 4). In the left hemisphere of LMTLE and RMTLE groups, cortical complexity was lower in the temporal, parietal, and occipital regions. In the right hemisphere, both MTLE groups had decreased cortical complexity in the temporal and occipital regions. In LMTLE, additional areas of reduced cortical complexity were found in the left frontal and right parietal regions.

Lack of Association between Cortical Thickness and Complexity

To determine if decreased cortical thickness was associated with reductions in cortical complexity, we performed correlation analysis of these 2 measurements. At each cortical point, the thickness was regressed against the corresponding lobar cortical complexity value. Only weak links were found between thinner cortex and lower cortical complexity in a small area of the right hemisphere of MTLE patients. However, this association did not survive after correction for multiple comparisons. No correlation was found in the control group. Therefore, there appears to be no straightforward relationship between these 2 measures of cerebral anatomy.

Decreased Cortical Thickness is Correlated with Longer Epilepsy Duration

In order to investigate the link between cortical thickness and clinical characteristics, regressions of thickness were performed against all the clinical characteristics listed in Table 1. Highly significant linkages were found relating longer duration of epilepsy to greater reductions in cortical thickness (Fig. 5). No significant correlation was found for age, age of seizure onset, gender, antiepileptic medication history, seizure frequency or initial precipitating injuries such as febrile seizure, central nervous system (CNS) infection, or head trauma. Longer seizure duration was correlated with decreased cortical thickness in the superior frontal parietal regions including the primary sensorimotor cortex and the parahippocampal gyrus ipsilateral to the side of seizure onset. Additional small regions of negative correlations were also found in the contralateral frontal region. Correcting for multiple comparisons, the ipsilateral hemisphere thickness decrease was significant ($P < 0.04$) but the contralateral hemisphere decrease was not significant ($P = 0.32$).

Asymmetry of Cortical Thickness in Epilepsy Groups

For clarity, the term "deficit" is defined as decrease in cortical thickness. In the LMTLE group (Fig. 6), a permutation test (which corrects for multiple comparisons) revealed 2 areas of asymmetry in the medial neocortex and no significant asymmetry for thickness was found in the lateral neocortex. Left greater than right deficits were found in the medial occipital region and right greater than left deficits were found in a small right frontal mesial region. In the RMTLE group (Fig. 6), right greater than left deficits were visualized in the frontal, perisylvian, and occipital regions ($P < 0.01$). Left greater than right deficits were seen mostly in the medial parietal occipital regions but also in 2 small areas in the lateral parietal and orbital frontal regions ($P < 0.01$). However, when we combined the 2 epilepsy groups and analyzed hemispheric asymmetry with respect to the side of seizure onset, we found no significant asymmetry between the 2 hemispheres.

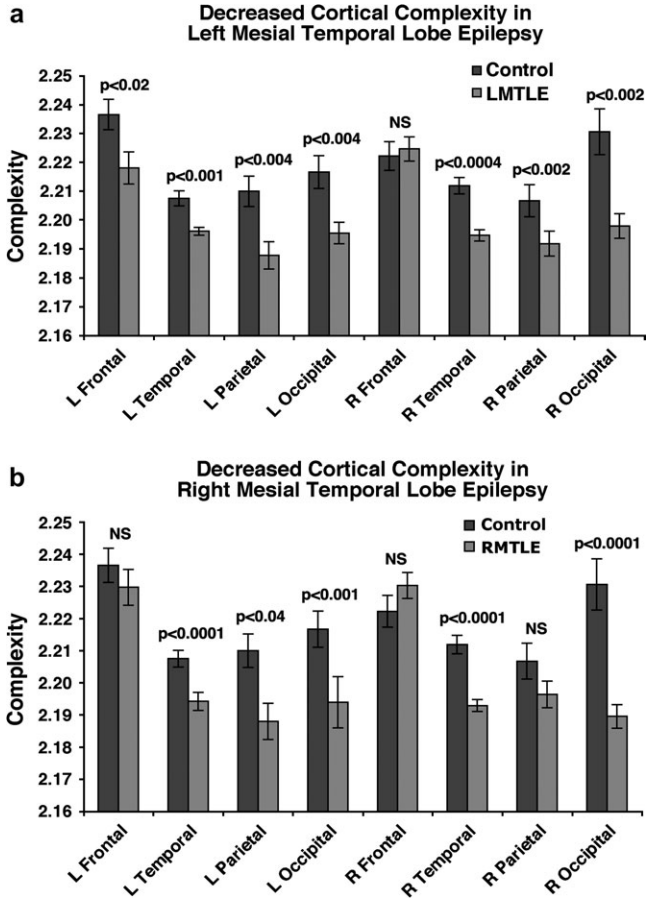

Figure 4. Cortical complexity is decreased in MTLE. The mean cortical complexity and standard errors are shown for each lobar region in MTLE subjects and in controls. In LMTLE (*a*), decreased cortical complexity was found in all lobar regions except the right frontal region. In RMTLE (*b*), decreased complexity was found in the bilateral temporal, occipital, and left parietal regions.

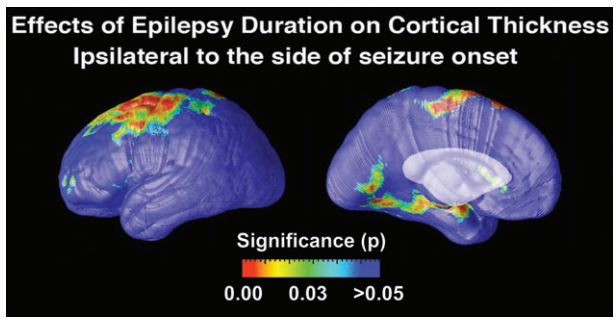

Figure 5. Cortical thickness correlated with seizure duration. Reduced cortical thickness is significantly correlated with longer seizure duration in the superior frontal parietal regions including the primary sensorimotor cortex and the parahippocampal gyrus ipsilateral to the side of seizure onset (red and yellow areas, $P < 0.04$). The contralateral effects were not found to be significant after correcting for multiple comparisons ($P = 0.32$).

Discussion

Because the MRI scans of the epilepsy patients were initially collected for clinical purposes, the control group was scanned with a different MRI protocol. To more directly address the effects of different scanner protocols, we rescanned a control

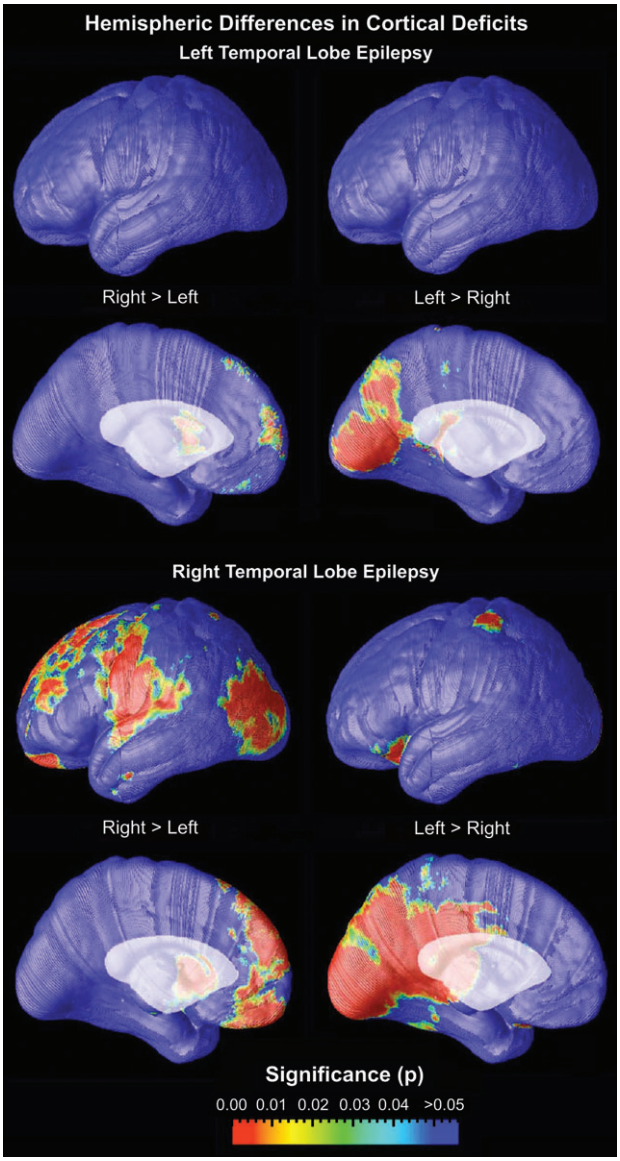

Figure 6. Maps of cortical thickness asymmetry in LMTLE and RMTLE. Deficit is defined as decrease in cortical thickness and areas of significance are denoted in red and yellow. In LMTLE, no hemispheric deficit asymmetry was found in the lateral cortex. In the medial cortex, the parietal occipital region showed left greater than right deficit, whereas the frontal region showed right greater than left deficit. In RMTLE, the right greater than left deficit was found in the frontal, perisylvian, and occipital regions of the lateral cortex. In the medical cortex, left greater than right deficit was found medial parietal occipital regions and right greater than left deficit was found in frontal regions. Thickness asymmetry in all these regions was found to be significant at $P < 0.01$.

subject from the original control cohort using the MTLE scanner protocol. An individual difference of 10% was found which, if systematic, would translate into an average group error estimate of 2.3% for mean gray matter volume in our 19 control subjects. Because the magnitude of mean reduction in MTLE groups' cortical thickness (up to 30% decrease compared with controls) is very large, the error caused by scanner effect is unlikely to contribute to the overall significance of our finding (and in fact would work against it). Further, the MTLE scanner protocol produced a slightly larger gray matter volume, which would bias, albeit only very slightly, against finding a reduction in the diseased group.

A large number of studies have been conducted in our laboratory using the same methods to map cortical thickness in normal healthy controls ($N = 40$, Thompson et al. 2005; $N = 78$, Narr et al. 2005; $N = 45$, Sowell et al. 2004; $N = 60$, Luders, Narr, Thompson, Rex, Jancke, et al. 2006; Luders, Narr, Thompson, Rex, Woods, et al. 2006). A remarkably similar pattern has emerged in the spatial distribution of cortical thickness in these control groups (Fig. 3*a*). Greatest thickness was found in the orbital frontal and lateral temporal regions followed by anterior frontal and perisylvian regions. The primary motor, sensory, and visual areas showed thinnest cortical thickness. This pattern was also apparent in a study of cortical development from childhood to early adulthood (Gogtay et al. 2004). These areas are in general agreement with postmortem measurements of cortical thickness by Von Economo (1929). However, the anterior temporal region is the thickest part of the cortex but this is not replicated in the average cortical thickness maps of our control group. The temporopolar region is partially surrounded by bone and tissue interfaces such as nasal sinuses, ear cavities, and perforated bone and thus is prone to susceptibility artifacts. Magnetic susceptibility differences between tissue/air and bone/tissue interfaces results in magnetic field gradients, which leads to intravoxel phase dispersion and image distortion. The difficulties in achieving good gray–white matter tissue contrast may lead to unusually low estimates for cortical thickness in the anteriormost part of the temporopolar region in our study. Cross-validation studies of different cortical thickness methods have also found high variability in this region (Kabani et al. 2001; Lerch and Evans 2005). Most investigators have therefore admitted that it is hard to obtain accurate cortical thickness estimates at the temporal lobe tip due to susceptibility gradients that complicate the ability of MRI to resolve boundaries in that restricted region.

In this study, cortical thickness maps and cortical complexity analyses provided a detailed characterization of the cortical deficit patterns in MTLE with HS. There were four main findings. First, we detected discrete sectors of reduced cortical thickness in bilateral frontal, temporal, and occipital lobes. Second, fractional dimension (complexity) measures of the human cerebral neocortex in 3D revealed that MTLE patients had significantly reduced cortical complexity in multiple lobar regions. Third, isolated decreased cortical thickness in the frontal parietal regions ipsilateral to the side of seizure onset was correlated with longer duration of epilepsy. Fourth, cortical asymmetry maps showed different regions of significant asymmetry in cortical thickness depending the side of seizure onset.

We selected patients with well-localized MTLE who had pathologically verified HS and had been seizure free for at least 2 years. Studying this group of patients who met strict criteria for MTLE with HS and known surgical outcomes allows us to better define typical structural changes in the neocortex associated with this epilepsy syndrome. Compared with VBM studies in TLE, our study in general showed similar patterns of cortical deficits (Keller et al. 2002; Bernasconi et al. 2004; Bonilha et al. 2004). Consistently, VBM studies have found gray matter reduction in various bilateral frontal regions. Both Keller's and Boniha's groups showed gray matter involvement in the bilateral parietal occipital regions, whereas Bernasconi and coworkers only found decrease in the occipital regions of left TLE patients. Different investigators have reported conflicting results in the temporal lobe neocortex with some suggesting increases in gray matter concentration (Keller et al. 2002), whereas others

have reported decreases in this region (Bernasconi et al. 2004; Bonilha et al. 2004). These discrepancies may result from different VBM tissue registration and segmentation techniques, as well as the fact that gray matter density measures are dependent on the curvature of the cortex, as well as on gray matter thickness. Keller et al. (2004) demonstrated that using "optimized" VBM, which incorporates additional spatial processing steps to improve image registration and conservation of tissue volumes after normalization, can increase sensitivity in detecting extrahippocampal structural abnormalities in TLE. In our present study, cortical pattern matching techniques allow the explicit matching of consistent neuroanatomical structures in the neocortex (i.e., sulcal landmarks and cortical surfaces) across subjects, thus enhancing the signal to noise for detecting group differences. In fact, the sulcal pattern alignment results in a higher-dimensional alignment of brain structure across subjects than is typically achievable using automated nonlinear registration approaches. Analyzing cortical thickness allows mapping of the actual depth of neocortex and meaningful quantitative measures of cerebral deficits can be visualized. A limitation of this technique is that it is solely focused on the neocortex, whereas VBM analysis can detect gray matter changes in subcortical structures as well as group differences in CSF and white matter.

Our findings clearly showed that structural abnormalities in patients with chronic unilateral MTLE extend beyond the affected ipsilateral hippocampus. The cortical deficits are primarily localized in the efferent neocortical limbic pathway. A study using MR tractography and diffusion tensor imaging (DTI) techniques in healthy subjects mapped not only the direct connectivity between the hippocampus and parahippocampal gyrus but also revealed reciprocal connections between parahippocampal gyrus and temporal, orbitalfrontal, extrastriate occipital lobes via lingual and fusiform gyri (Powell et al. 2004). A similar limbic neocortical network has also been demonstrated in patients with complex partial seizures using interictal and ictal single photon emissions computed tomography (Van Paesschen et al. 2003). The cortical areas implicated in these studies are remarkably similar to the cortical deficit patterns found in our study.

All the MTLE patients have drug-resistant epilepsy and it is important to evaluate the effects of disease burden on cortical deficits. Epilepsy disease burden can be quantified in terms of duration of epilepsy, seizure frequency, severity of the seizure type (i.e., generalized tonic clonic seizures versus complex partial seizures), and all of these factors are potential contributors to the distributed atrophy pattern. When we correlated clinical factors with cortical thickness, significant linkages were found relating longer duration of epilepsy with reduced cortical thickness in the frontal parietal region only ipsilateral to the side of seizure onset. The frontal parietal region surrounding the central sulcus is integral in generating motor phenomena during complex partial and secondary generalized seizures. It is possible that longer duration of illness will lead to more frequent secondarily generalized seizures, thus causing progressive atrophy in this region. VBM studies also found correlations between decreased gray matter density in this region and seizure duration but their results were bilateral (Keller et al. 2002; Bonilha et al. 2006). Although patients with higher seizure frequency have more greatly impaired cognitive functions and successful surgical treatment may arrest progression or improve cognition, this factor was not associated with greater cortical deficits in our study. Liu et al. (2003) in a longitudinal study of patients with chronic and newly diagnosed epilepsy also did not find any correlation. In addition, they did not show greater atrophy in patients with generalized seizures when compared with complex partial seizures. However, there is some indirect evidence that patients with generalized seizures have greater disease burden. In a multicenter study for epilepsy surgery, the presence of generalized tonic clonic seizure was a poor prognostic factor for successful surgical treatment in MTLE, suggesting that generalized seizure involves a widespread epileptogenic zone that may be less amenable to surgical treatment (Spencer et al. 2005).

Cortical deficits found in this study may also result from cerebral damage due to an initial injury; chronic progression of the damage caused by the initial injury; or chronic exposure to antiepileptic drugs (Pitkanen and Sutula 2002; Liu et al. 2003). Initial precipitating injury such as febrile seizures, head trauma, or CNS infection may cause acute structural damage, neuronal reorganization, and development of chronic epileptogenesis (Mathern et al. 1995; Santhakumar et al. 2001; O'Brien et al. 2002; Theodore et al. 2003). In animal models, exposure to antiepileptic drugs can cause apoptotic neurodegeneration in the developing brain (Bittigau et al. 2002). Several studies have found that increase in exposure to antiepileptic drugs is associated with greater degree of brain atrophy independent of seizure control (De Marcos et al. 2003; Liu et al. 2003). We attempted to correlate these clinical factors (Table 1) to cortical thickness and found no clear association. This study may be underpowered to detect the subtle nature of cerebral deficits associated with these variables and additional study of a larger population is warranted to further define contributions of these factors to the distributed pattern of brain atrophy.

In addition to cortical thickness, we also investigated gyrification abnormalities in MTLE in 3D space. Analysis of cortical folding patterns using fractal geometry in serial 2D sections has been applied to epilepsy. Cook et al. (1995) used this technique to evaluate cortical patterns in frontal and TLE patients with apparently normal brain MRI. Nine of the 16 frontal lobe patients had reductions in fractal dimension of the gray/white matter interface contour in 2D coronal and axial planes, whereas TLE patients did not show any significant alteration. Unfortunately, 2D measures of fractal dimension vary depending on the direction in which the brain scan is sliced and whether the analysis was calculated on the whole brain rather than after parcellation of lobes. We calculated cortical complexity for the cortical surface of each lobe in 3D, resulting in measures that are independent of brain size and orientation (see Thompson et al. 2005 for an explanation). Cortical complexity was significantly reduced in multiple lobar regions in both MTLE groups.

Malformations of cortical development (MCD) are commonly associated with abnormal gyral features (Guerrini et al. 2003). In this study, patients with MCD on visual inspection of the MRI were excluded from the study. Therefore, the decreased cortical complexity observed in our study is unlikely to be due to visually apparent MCD such as lissencephaly or pachygyria. However, microscopic MCD such as cortical dysplasia exists in about 40% MTLE with HS and may lead to gyral simplification (Guerrini et al. 2003; Kalnins et al. 2004). Although we excluded patients with microscopic cortical dysplasia on postoperative surgical temporal lobe specimens, the standard en-bloc anteriomesial temporal resection only

provided a limited cortical area for pathological inspection (Spencer et al. 1984). It is possible that subtle MCD exists in other unresected neocortical regions. Pathological features of cortical dysplasia observed included diffuse architectural disorganization, neuronal cytomegaly, increased number of molecular layer neurons, balloon cells, gray matter heterotopia, and neuronal glial clustering (Prayson and Frater 2003). Using DTI with tractography, Lee et al. (2004) visualized decreased subcortical connectivity in the subcortex and deep white matter underlying areas of focal cortical dysplasia. In the normal cortex contralateral to the lesion, the longitudinal fibers reached each gyri with a branching pattern. However, the lesional side failed to show connectivity between the white matter and the dysplastic cortex. Perturbation in connections between cortical regions may alter the mechanical tension that has been hypothesized as required for normal development of cortical folding (Van Essen 1997). Thus, underlying neuronal connectivity significantly influences gyral patterns, and these dysplastic subcortical lesions may cause alteration in cortical gyri.

It is intriguing to evaluate whether cortical complexity and thickness are related. In our previous study of Williams syndrome, significant association between thicker cortex and greater complexity was only found in the right hemisphere of healthy controls but no association was found in the Williams syndrome group (Thompson et al. 2005). Interestingly, although Williams syndrome subjects had regionally increased cortical thickness, the overall gray matter volume was decreased and hemispheric cortical complexity was increased. In our current study of epilepsy patients, there was also no strong evidence that cortical thickness and complexity were correlated. Although cortical dysplasia has been associated with gyral abnormalities, it is not associated with reduced cortical thickness. Thickened cortex and blurring of the gray–white matter junction are features most commonly seen on MRI (Guerrini et al. 2003). Therefore, it is unlikely that one measure of cortical anatomy (i.e., complexity) is simply an epiphenomenon of the other measure (i.e., thickness) or vice versa.

Even though both MTLE groups showed bilateral reduction in cortical thickness when compared with healthy controls, asymmetry maps revealed markedly different patterns of cortical deficits in these 2 groups. Asymmetry maps are a within-group analysis. The first study examines the differences in cortical thickness between the right and left hemisphere separately in each epilepsy group. Luders, Narr, Thompson, Rex, Jancke, et al. (2006) showed that in normal healthy controls (N = 60), the right lateral hemisphere and medial frontal regions in general showed a normal asymmetry of 5–10% decrease in cortical thickness compared with the left side. In the medial parietal occipital regions, there is a normal asymmetry of decrease cortical thickness on left hemisphere compared with the right. In our LMTLE group, no significant asymmetry was found in the lateral neocortex, whereas the medial asymmetry pattern was preserved compared with Luders' control population (Fig. 6). In our RMTLE group, the asymmetry maps demonstrated a right greater than left deficit in the lateral frontal, perisylvian, and occipital regions, whereas the medial hemispheric difference was again similar to Luders controls (Fig. 6). When an additional analysis was performed to measure hemispheric asymmetry with respect to the side of seizure onset, no significant asymmetry was found between the 2 hemispheres. This is an unexpected finding because greater disease burden is expected on the side where seizures originated. We expected that pooling the data from the 2 groups would increase the power to detect anatomical differences between the 2 hemispheres, as would be the case if the pathological contribution to asymmetry was substantially greater than the normal underlying asymmetry. However, collapsing across the 2 groups may have added unexpected anatomical noise, making the hemispheric differences more difficult to detect. In normal subjects' brains, there are baseline hemispheric asymmetries in which right lateral hemispheric and medial frontal regions and left medial parietal occipital regions have been shown to exhibit a decreased cortical thickness when compared with contralateral homologous regions (Luders, Narr, Thompson, Rex, Jancke, et al. 2006). Because brains exhibit baseline asymmetries, the epileptic process may further modify these asymmetries in the opposite directions depending on the side of seizure onset. These effects may in certain brain regions accentuate baseline asymmetry and in other regions cancel out baseline asymmetry. These images were transformed across the midline plane in order to keep the side of seizure onset consistent. The differential effects of epilepsy on each hemisphere may have added anatomical variance, leading to a failure to detect hemispheric differences. For example, when collapsing across side of seizure onset intersubject anatomical variance is added, as the normal asymmetry will have been added in one direction for 15 subjects and in the other direction for the other 15 subjects. Clearly, the outcome of this experiment depends on whether the mean pathological contribution to asymmetry is sufficiently large to outweigh the added variance in normally occurring asymmetries that are added in opposite directions when data are pooled by side of seizure onset. Because this is a surprising finding, we will follow up with cross-validation studies to evaluate this hypothesis in future samples that are large enough to separate the normal and pathological components of asymmetry.

It is clear that this epilepsy syndrome is associated with asymmetric involvement of the lateral neocortex depending on the side of the seizure onset with minimal effects on the medial neocortex. One hypothesis is that recurrent seizures resulted in differences in cortical asymmetry in these 2 epilepsy groups. Seizures that originate in the left mesial temporal regions may cause greater left hemisphere deficits and thus obliterate the right greater than left deficit pattern seen in the lateral neocortex of healthy controls. The RMTLE group showed a right greater than left deficit pattern in the lateral neocortex. Seizures that originate in the right mesial temporal regions may cause greater right hemisphere damage and may further enhance the right greater than left deficit pattern in the lateral neocortex of normal controls. Alternatively, these asymmetry maps may merely reflect preexisting structure deficits associated with each epilepsy population. Each group may have a preexisting preponderance of hemisphere deficits ipsilateral to the side of seizure onset. In familial TLE with aura, an autosomal dominant focal epilepsy caused by a mutation on LGI1 gene on chromosome 10q, visual inspection of the brain MRI scans revealed malformation and enlargement of the left lateral temporal lobes (Kobayashi et al. 2003). This anatomical asymmetry was also correlated with functional abnormality. The patients with this genetic form of TLE also had a reduction in the long latency auditory evoke potentials on the left side when compared with normal controls (Brodtkorb et al. 2005). In a recent functional MRI study, Berl et al. (2005) investigated the degree of left hemisphere language dominance in patients with left and right

side seizure onset. Patients with left hemisphere seizure onset had a lesser degree of left hemisphere language dominance (leftward asymmetry index < 0.20) when compared with right side onset and normal controls. This supports the hypothesis that the seizures or their remote symptomatic etiology had adverse effects on left side language processing and may have caused a partial shift of language processing to the contralateral homologous regions. Our asymmetry maps (Fig. 6) also corroborate these differences in asymmetry anatomically. The left side seizure onset patients showed no significant asymmetry in the lateral neocortex, whereas the right side seizure onset patients showed areas of asymmetric decrease in cortical thickness mostly in lateral areas of the right hemisphere.

In summary, cortical thickness analysis using cortical pattern matching allows precise quantitative characterization of deficit patterns in a group of patients who met strict criteria for MTLE with HS with seizure-free surgical outcome. These average maps of cortical deficits revealed group-specific features not apparent in an individual MRI scan. Patients with MTLE with HS who have good surgical outcome may represent an anatomically similar group that has common disease-specific patterns of structural abnormalities. In a randomized study of surgery for MTLE, 36% patients of patients continued to have seizures after surgical treatment (Wiebe et al. 2001). Previous quantitative MRI studies have shown that greater extrahippocampal structural abnormalities are associated with poor surgical and neuropsychological outcome in this epilepsy syndrome (Sisodiya et al. 1995; Baxendale et al. 1999). The pattern of anatomical deviation from the disease-specific regions of abnormality may contribute to individual probability of seizure freedom and help predict surgical outcome. To test this hypothesis, our next study will prospectively compute anatomical differences for individual patients with MTLE and HS, relative to the disease-specific features, and correlate these differences with postsurgical seizure outcome. We also plan to perform cross-validation studies to evaluate the reproducibility of the distributed anatomical deficits in the same subjects across time and with different scanner protocols.

Notes

We thank Sandra Dewar, RN, MS for conducting patient telephone interviews and maintaining the epilepsy database. This work was funded by grants from the Epilepsy Foundation Clinical Research Training Fellowship, National EpiFellows Foundation Fritz E. Dreifuss Award (to J.J.L. and J.E.), the National Institute for Biomedical Imaging and Bioengineering (NIBIB), the National Center for Research Resources (NCRR), the National Institute on Aging (to P.T.: R21 EB01651, R21 RR019771, P50 AG016570), the National Institute of Neurological Disorders and Stroke (NINDS) (to J.E.: NS02808, NS033310), and by the following grants from NCRR, NIBIB, NINDS, and National Institute of Mental Health: PO1 EB001955, U54 RR021813, MO1 RR000865, and P41 RR13642 (to A.W.T.). *Conflict of Interest*: None declared.

Address correspondence to Jack J. Lin, MD, Department of Neurology, University of California, Irvine, 101 The City Dr. South, Bldg. 22C, 2nd Floor, Rt. 13, Orange, CA 92868, USA. Email: linjj@uci.edu.

References

Annese J, Pitiot A, Toga AW. 2002. 3D cortical thickness maps from histological volume. Neuroimage. 13:S858.

Armstrong E, Schleicher A, Omran H, Curtis M, Zilles K. 1995. The ontogeny of human gyrification. Cereb Cortex. 5:56–63.

Babb TL, Lieb JP, Brown WJ, Pretorius J, Crandall PH. 1984. Distribution of pyramidal cell density and hyperexcitability in the epileptic human hippocampal formation. Epilepsia. 25:721–728.

Baxendale SA, Sisodiya SM, Thompson PJ, Free SL, Kitchen ND, Stevens JM, Harkness WF, Fish DR, Shorvon SD. 1999. Disproportion in the distribution of gray and white matter: neuropsychological correlates. Neurology. 52:248–252.

Berl MM, Balsamo LM, Xu B, Moore EN, Weinstein SL, Conry JA, Pearl PL, Sachs BC, Grandin CB, Frattali C, et al. 2005. Seizure focus affects regional language networks assessed by fMRI. Neurology. 65:1604–1611.

Bernasconi N, Bernasconi A, Caramanos Z, Antel SB, Andermann F, Arnold DL. 2003. Mesial temporal damage in temporal lobe epilepsy: a volumetric MRI study of the hippocampus, amygdala and parahippocampal region. Brain. 126:462–469.

Bernasconi N, Duchesne S, Janke A, Lerch J, Collins DL, Bernasconi A. 2004. Whole-brain voxel-based statistical analysis of gray matter and white matter in temporal lobe epilepsy. Neuroimage. 23:717–723.

Bittigau P, Sifringer M, Genz K, Reith E, Pospischil D, Govindarajalu S, Dzietko M, Pesditschek S, Mai I, Dikranian K, et al. 2002. Antiepileptic drugs and apoptotic neurodegeneration in the developing brain. Proc Natl Acad Sci USA. 99:15089–15094.

Blanton RE, Levitt JL, Thompson PM, Capetillo-Cunliffe LF, Sadoun T, Williams T, McCracken JT, Toga AW. 2000. Mapping cortical variability and complexity patterns in the developing human brain. Psychiatry Res. 107:29–43.

Bonilha L, Rorden C, Appenzeller S, Carolina Coan A, Cendes F, Min Li L. 2006. Gray matter atrophy associated with duration of temporal lobe epilepsy. Neuroimage. 32(3):1070–1079.

Bonilha L, Rorden C, Castellano G, Pereira F, Rio PA, Cendes F, Li LM. 2004. Voxel-based morphometry reveals gray matter network atrophy in refractory medial temporal lobe epilepsy. Arch Neurol. 61:1379–1384.

Brodtkorb E, Steinlein OK, Sand T. 2005. Asymmetry of long-latency auditory evoked potentials in LGI1-related autosomal dominant lateral temporal lobe epilepsy. Epilepsia. 46:1692–1694.

Bullmore ET, Suckling J, Overmeyer S, Rabe-Hesketh S, Taylor E, Brammer MJ. 1999. Global, voxel, and cluster tests, by theory and permutation, for a difference between two groups of structural MR images of the brain. IEEE Trans Med Imaging. 18:32–42.

Cook MJ, Free SL, Manford MR, Fish DR, Shorvon SD, Stevens JM. 1995. Fractal description of cerebral cortical patterns in frontal lobe epilepsy. Eur Neurol. 35:327–335.

De Marcos FA, Ghizoni E, Kobayashi E, Li LM, Cendes F. 2003. Cerebellar volume and long-term use of phenytoin. Seizure. 12:312–315.

Fischl B, Dale AM. 2000. Measuring the thickness of the human cerebral cortex from magnetic resonance images. Proc Natl Acad Sci USA. 97:11050–11055.

Gogtay N, Giedd JN, Lusk L, Hayashi KM, Greenstein D, Vaituzis AC, Nugent TF, 3rd, Herman DH, Clasen LS, Toga AW, et al. 2004. Dynamic mapping of human cortical development during childhood through early adulthood. Proc Natl Acad Sci USA. 101:8174–8179.

Gu X, Wang YL, Chan T, Thompson PM, Yau ST. 2003. Genus zero conformal mapping and its application to brain surface mapping. In: Taylor CJ, Noble JA, editors. 18th International Conference on Information Processing in Medical Imaging (IPMI2003): Lecture Notes in Computer Science. Vol. 2732. New York: Springer. p 172–184.

Guerrini R, Sicca F, Parmeggiani L. 2003. Epilepsy and malformations of the cerebral cortex. Epileptic Disord 5(Suppl 2):S9–S26.

Hammers A, Koepp MJ, Labbe C, Brooks DJ, Thom M, Cunningham VJ, Duncan JS. 2001. Neocortical abnormalities of [11C]-flumazenil PET in mesial temporal lobe epilepsy. Neurology. 56:897–906.

Hayashi KM, Thompson PM, Mega MS, Zoumalan CI, Dittmer SS. 2002. Medial hemispheric surface gyral pattern delineation in 3D: surface protocol, http://www.loni.ucla.edu/khayashi/Public/medial_surface/.

Henry TR, Mazziotta JC, Engel J, Jr. 1993. Interictal metabolic anatomy of mesial temporal lobe epilepsy. Arch Neurol. 50:582–589.

Jones SE, Buchbinder BR, Aharon I. 2000. Three-dimensional mapping of cortical thickness using Laplace's equation. Hum Brain Mapp. 11:12–32.

Kabani N, Le Goualher G, MacDonald D, Evans AC. 2001. Measurement of cortical thickness using an automated 3-D algorithm: a validation study. Neuroimage. 13:375–380.

Kalnins RM, McIntosh A, Saling MM, Berkovic SF, Jackson GD, Briellmann RS. 2004. Subtle microscopic abnormalities in hippocampal sclerosis

do not predict clinical features of temporal lobe epilepsy. Epilepsia. 45:940–947.
Keller SS, Wieshmann UC, Mackay CE, Denby CE, Webb J, Roberts N. 2002. Voxel based morphometry of grey matter abnormalities in patients with medically intractable temporal lobe epilepsy: effects of side of seizure onset and epilepsy duration. J Neurol Neurosurg Psychiatry. 73:648–655.
Keller SS, Wilke M, Wieshmann UC, Sluming VA, Roberts N. 2004. Comparison of standard and optimized voxel-based morphometry for analysis of brain changes associated with temporal lobe epilepsy. Neuroimage. 23:860–868.
Kiselev VG, Hahn KR, Auer DP. 2003. Is the brain cortex a fractal? Neuroimage. 20:1765–1774.
Kobayashi E, Santos NF, Torres FR, Secolin R, Sardinha LA, Lopez-Cendes I, Cendes F. 2003. Magnetic resonance imaging abnormalities in familial temporal lobe epilepsy with auditory auras. Arch Neurol. 60:1546–1551.
Kruggel F, Bruckner MK, Arendt T, Wiggins CJ, von Cramon DY. 2001. Analyzing the neocortical fine structure. In: Insana MF, Leahy RM, editors. Information processing in medical imaging. New York: Springer Press. p. 239–245.
Lee SK, Kim DI, Mori S, Kim J, Kim HD, Heo K, Lee BI. 2004. Diffusion tensor MRI visualizes decreased subcortical fiber connectivity in focal cortical dysplasia. Neuroimage. 22:1826–1829.
Lerch JP, Evans AC. 2005. Cortical thickness analysis examined through power analysis and a population simulation. Neuroimage. 24:163–173.
Liu RS, Lemieux L, Bell GS, Hammers A, Sisodiya SM, Bartlett PA, Shorvon SD, Sander JW, Duncan JS. 2003. Progressive neocortical damage in epilepsy. Ann Neurol. 53:312–324.
Luders E, Narr KL, Thompson PM, Rex DE, Jancke L, Toga AW. 2004. Gender differences in cortical complexity. Nat Neurosci. 7:799–800.
Luders E, Narr KL, Thompson PM, Rex DE, Jancke L, Toga AW. 2006. Hemispheric asymmetries in cortical thickness. Cereb Cortex. 16:1232–1238.
Luders E, Narr KL, Thompson PM, Rex DE, Woods RP, Deluca H, Jancke L, Toga AW. 2006. Gender effects on cortical thickness and the influence of scaling. Hum Brain Mapp. 27:314–324.
MacDonald D, Kabani N, Avis D, Evans AC. 2000. Automated 3-D extraction of inner and outer surfaces of cerebral cortex from MRI. Neuroimage. 12:340–356.
Mathern GW, Pretorius JK, Babb TL. 1995. Influence of the type of initial precipitating injury and at what age it occurs on course and outcome in patients with temporal lobe seizures. J Neurosurg. 82:220–227.
Miller MI, Massie AB, Ratnanather JT, Botteron KN, Csernansky JG. 2000. Bayesian construction of geometrically based cortical thickness metrics. Neuroimage. 12:676–687.
Moran NF, Lemieux L, Kitchen ND, Fish DR, Shorvon SD. 2001. Extrahippocampal temporal lobe atrophy in temporal lobe epilepsy and mesial temporal sclerosis. Brain. 124:167–175.
Narr KL, Bilder RM, Toga AW, Woods RP, Rex DE, Szeszko PR, Robinson D, Sevy S, Gunduz-Bruce H, Wang YP, DeLuca H, Thompson PM. 2005. Mapping cortical thickness and gray matter concentration in first episode schizophrenia. Cereb Cortex. 15(6):708–719.
Nichols TE, Holmes AP. 2002. Nonparametric permutation tests for functional neuroimaging: a primer with examples. Hum Brain Mapp. 15:1–25.
O'Brien TJ, Moses H, Cambier D, Cascino GD. 2002. Age of meningitis or encephalitis is independently predictive of outcome from anterior temporal lobectomy. Neurology. 58:104–109.
Ono M, Kubik S, Abernathey C. 1990. Atlas of the cerebral sulci. Stuttgart, Germany: Thieme.
Oyegbile TO, Dow C, Jones J, Bell B, Rutecki P, Sheth R, Seidenberg M, Hermann BP. 2004. The nature and course of neuropsychological morbidity in chronic temporal lobe epilepsy. Neurology. 62:1736–1742.
Pitkanen A, Sutula TP. 2002. Is epilepsy a progressive disorder? Prospects for new therapeutic approaches in temporal-lobe epilepsy. Lancet Neurol. 1:173–181.
Powell HWR, Guye M, Parker GJM, Symms MR, Boulby P, Koepp MJ, Barker GJ, Duncan JS. 2004. Noninvasive in vivo demonstration of the connections of the human parahippocampal gyrus. Neuroimage. 22:740–747.
Prayson RA, Frater JL. 2003. Cortical dysplasia in extratemporal lobe intractable epilepsy: a study of 52 cases. Ann Diagn Pathol. 7:139–146.
Rakic P. 1988. Specification of cerebral cortical areas. Science. 241:170–176.
Santhakumar V, Ratzliff AD, Jeng J, Toth Z, Soltesz I. 2001. Long-term hyperexcitability in the hippocampus after experimental head trauma. Ann Neurol. 50:708–717.
Shattuck DW, Sandor-Leahy SR, Schaper KA, Rottenberg DA, Leahy RM. 2001. Magnetic resonance image tissue classification using a partial volume model. Neuroimage. 13:856–876.
Sisodiya SM, Free SL, Stevens JM, Fish DR, Shorvon SD. 1995. Widespread cerebral structural changes in patients with cortical dysgenesis and epilepsy. Brain 118(Pt 4):1039–1050.
Sowell ER, Thompson PM, Leonard CM, Welcome SE, Kan E, Toga AW. 2004. Longitudinal mapping of cortical thickness and brain growth in normal children. J Neurosci. 24:8223–8231.
Sowell ER, Thompson PM, Rex D, Kornsand D, Tessner KD, Jernigan TL, Toga AW. 2002. Mapping sulcal pattern asymmetry and local cortical surface gray matter distribution in vivo: maturation in perisylvian cortices. Cereb Cortex. 12:17–26.
Spencer DD, Spencer SS, Mattson RH, Williamson PD, Novelly RA. 1984. Access to the posterior medial temporal lobe structures in the surgical treatment of temporal lobe epilepsy. Neurosurgery. 15:667–671.
Spencer SS, Berg AT, Vickrey BG, Sperling MR, Bazil CW, Shinnar S, Langfitt JT, Walczak TS, Pacia SV. 2005. Predicting long-term seizure outcome after resective epilepsy surgery: the multicenter study. Neurology. 65:912–918.
Theodore WH, DeCarli C, Gaillard WD. 2003. Total cerebral volume is reduced in patients with localization-related epilepsy and a history of complex febrile seizures. Arch Neurol. 60:250–252.
Thompson PM, Hayashi KM, de Zubicaray G, Janke AL, Rose SE, Semple J, Herman D, Hong MS, Dittmer SS, Doddrell DM, et al. 2003. Dynamics of gray matter loss in Alzheimer's disease. J Neurosci. 23:994–1005.
Thompson PM, Hayashi KM, Simon SL, Geaga JA, Hong MS, Sui Y, Lee JY, Toga AW, Ling W, London ED. 2004. Structural abnormalities in the brains of human subjects who use methamphetamine. J Neurosci. 24:6028–6036.
Thompson PM, Hayashi KM, Sowell ER, Gogtay N, Giedd JN, Rapoport JL, de Zubicaray GI, Janke AL, Rose SE, Semple J, et al. 2004. Mapping cortical change in Alzheimer's disease, brain development, and schizophrenia, special issue on mathematics in brain imaging. Neuroimage. 23(Suppl 1):S2–S18.
Thompson PM, Lee AD, Dutton RA, Geaga JA, Hayashi KM, Eckert MA, Bellugi U, Galaburda AM, Korenberg JR, Mills DL, et al. 2005. Cortical complexity and thickness are increased in Williams syndrome. J Neurosci. 25(16):4146–4158.
Thompson PM, Schwartz C, Lin RT, Khan AA, Toga AW. 1996. Three-dimensional statistical analysis of sulcal variability in the human brain. J Neurosci. 16:4261–4274.
Van Essen DC. 1997. A tension-based theory of morphogenesis and compact wiring in the central nervous system. Nature. 385:313–318.
Van Paesschen W, Dupont P, Van Driel G, Van Billoen H, Maes A. 2003. SPECT perfusion changes during complex partial seizures in patients with hippocampal sclerosis. Brain. 126:1103–1111.
Von Economo CV. 1929. The cytoarchitectonics of the human cerebral cortex. London: Oxford Medical Publications.
Wiebe S, Blume WT, Girvin JP, Eliasziw M. 2001. A randomized, controlled trial of surgery for temporal-lobe epilepsy. N Engl J Med. 345:311–318.
Wright IC, McGuire PK, Poline JB, Travere JM, Murray RM, Frith CD, Frackowiak RS, Friston KJ. 1995. A voxel-based method for the statistical analysis of gray and white matter density applied to schizophrenia. Neuroimage. 2:244–252.
Yezzi A, Prince J. 2001. A PDE approach for measuring tissue thickness. In: Computer vision and pattern recognition. Berlin: Springer. p. 213–220
Zilles K, Armstrong E, Schleicher A, Kretschmann HJ. 1988. The human pattern of gyrification in the cerebral cortex. Anat Embryol (Berl). 179:173–179.